Faraday Discussions

ARTICLE

Structural analysis of heavy oil fractions after hydrodenitrogenation by high-resolution tandem mass spectrometry and ion mobility spectrometry

Received 00th January 20xx,
Accepted 00th January 20xx

DOI: 10.1039/C8FD00239H

www.rsc.org/

Johann Le Maître[a,b,c], Marie Hubert-Roux[a,c], Benoit Paupy[b,c], Sabrina Marceau[b,c], Christopher Rüger[a], Carlos Afonso[a,c], Pierre Giusti[b,c]

Heavy petroleum fractions such as vacuum gas oils (VGOs) are structurally and compositionally highly complex mixtures. Nitrogen species which have a significant impact on the subsequent refining processes are generally removed by the hydrodenitrogenation (HDN) catalytic process. The purpose of this study was to identify and characterize compounds that are refractory to the HDN process. This may allow examining the effectiveness of a vacuum distillate hydrotreatment catalytic bed in removing nitrogen-containing compounds before the cracking step. . Three different VGO fractions of the same oil before and after HDN processes were analysed in ESI(+) by FTICR mass spectrometry and ion mobility spectrometry - mass spectrometry (IMS-MS); in particular compounds containing basic nitrogen, such as quinoline and isoquinoline. Ultra-high resolution FTICR mass spectrometry provides a sufficiently high mass resolution power to resolve different compounds and attribute to each ion a unique molecular formula. Information on the isomeric content was obtained by use of tandem mass spectrometry (MS/MS) and IMS-MS. The evolution of the fragmentation of the N1 class compounds as a function of collision energy allowed the identification of the molecular nucleus raw formula. From the IMS-MS experiments, it appeared clearly that based on IMS peak width, lower isomeric dispersity was obtained after the HDN process and based on drift time and collision cross section determination, species presenting longer alkyl branches are the molecules most refractory to the HDN process.

Introduction

Heavy petroleum fractions such as vacuum gas oil (VGO) are some of the most complex mixtures in nature, containing tens of thousands of different organic compounds.[1, 2] They consist of saturated and aromatic hydrocarbons, heteroatomic molecules containing mainly nitrogen, oxygen, and sulfur, and organometallic compounds, such as vanadyl and nickel porphyrins.[3-5] The presence of heteroelements drastically affect the activity of the conversion catalyst. Therefore, removal of nitrogen, sulfur and metals is essential for petroleum catalytic hydrocracking process. This is generally achieved by use of hydrodemetallation (HDM), hydrodesulfurization (HDS), hydrodenitrogenation (HDN) steps with catalytic beds in the hydrotreatment process.[6-15] In particular, nitrogen containing species have a significant impact on refining processes due to the poisoning of HDS catalysts.[14] Hydrodenitrogenation does not occur directly at unsaturated rings, meaning that unsaturated nitrogen-containing heterocycles must first be saturated before the carbon-nitrogen cleavage can occur.[14]

Refractory compounds that resist catalytic hydrodenitrogenation, under given process conditions, are targeted in this study. Knowledge of the molecular composition has become an important challenge in analytical development, particularly in the case of heavy petroleum fractions evaluation. The determination of the quantity and structure of molecules containing heteroatoms is essential for these catalytic hydrotreating processes.[16] Due to the complexity of petroleum, ultra-high resolution Fourier transform ion cyclotron resonance mass spectrometry (FTICR MS) is an appropriate analytical method[17-19] affording exhaustive molecular formula attribution.[20-21] However mass spectrometry alone cannot separate isomers although differences in isomeric content can yield to different molecular properties. Another dimension of separation is required to obtain information on isomeric content.

[a]*Normandie Université, COBRA, UMR 6014 et FR 3038; Université de Rouen; INSA de Rouen; CNRS, IRCOF, Mont Saint Aignan Cedex, France*
[b]*TOTAL Refining & Chemicals, Total Research & Technology Gonfreville, BP 27, 76700 Harfleur, France.*
[c]*CNRS Joint Laboratory C2MC, Complex Matrices Molecular Characterization - CNRS (France) BP 27, 76700 Harfleur, France.*
† Footnotes relating to the title and/or authors should appear here.
Electronic Supplementary Information (ESI) available: [details of any supplementary information available should be included here]. See DOI: 10.1039/x0xx00000x

This can be afforded by chromatographic separation,[1] ion mobility spectrometry (IMS)[22] or tandem mass spectrometry (MS/MS).[23] For MS/MS, ions are first selected in the quadrupole and subsequently dissociated, *e.g.*, by collision-induced dissociation (CID) in a collision cell[23-26] before their detection. It has been demonstrated that weak σ-bonds of alkyl chains connected to an aromatic core structure can be cleaved by CID.[27] Many compositional and structural questions are being investigated in heavy crude oil fractions, such as vacuum gas oil (VGO), bitumen and asphaltene by Kekäläinen et al.[27], Wittrig et al.[23], Chacón-Patiño et al.[28-31], and petroleum emulsion interfacial materials by Lalli et al.[24] Research on their chemical composition and physical structures includes examining the heteroatom distribution and the structural conformation by the single and multiple nucleus structures with respect to their composition. Two structural models exist concerning the nuclei of oil compounds: archipelago type (a set of nuclei close to each other and bridged by linkers), and island type (a single nucleus).[28, 29] Among the different types of oil characterization diagrams issued from FTICR data, the most commonly used is the mapping representing the number of double bond equivalent as a function of the carbon number (DBE/C#) for a given class of heteroatoms.[32-34] These represent the "molecular fingerprint" of a given sample. This type of map makes it also possible to visualize the thousands of elemental compositions revealed for a given class, and thus to identify the structural compositions of the various compounds in the oil samples. It is possible to differentiate structural families by studying DBE/C# maps from MS/MS spectra.[29, 30, 35, 36]

It has been shown that ion mobility spectrometry coupled to mass spectrometry (IMS-MS) is a valuable tool for the characterization of complex mixtures such as petroleum products. Besides partial separation of isomers, it gives access to the collision cross section (CCS) that is a descriptor of the ion structure.[37-40] In practice owing to the very high number of isomers present for one particular molecular formula, one will not expect to obtain separation of the isomeric species but generally a broad unresolved signal. The measured drift time of this signal is related to the average ion CCS whereas the peak width is related to the isomeric content.[37] As in the case of a structural determination by CID, many studies are being conducted on the use of IMS-MS such as the characterization of crude oil.[22]

The ESI source allows selective ionization of basic or acidic compounds. In petroleum samples, this leads to the detection of compounds containing basic (*e.g.*, quinolines)[15, 41] or neutral nitrogen (*e.g.*, carbazole)[42, 43] in positive and negative ion mode respectively and, thus, reducing the overall observed complexity.[44] The electrospray ionization being discriminating, the nitrogen-containing ions are found to be the most intense signals in both, positive and negative ion detection mode. The objective of this work is to characterize basic nitrogen-containing compounds that are refractory to the catalytic processes. A feed and effluents from HDN processes were analyzed by ultra-high-resolution FTICR and IMS-MS in positive mode.

Experimental

Sample preparation

Three samples (Vacuum gas oil with 1000 ppm N and two effluents with 70 and 10 ppm N) were supplied by Total Research and Technology (Gonfreville, France). Samples were solubilized in toluene and further diluted in methanol/toluene (50/50 v/v) to a final concentration of 1 mg.mL^{-1}. The diluted solution was spiked with 1% formic acid for the positive mode analyses.

Instrumentation

A hybrid quadrupole FTICR instrument (solariX XR, Bruker Daltonics, Bremen, Germany) equipped with a 12 T superconducting magnet was operated in the positive electrospray mode. Mass spectra were acquired over a mass range of *m/z* 147-1,300 for 400 scans for broadband experiments and 20 and 50 scans for isolation and fragmentation spectra, respectively. The signal was digitalized with 8 M points resulting in a transient length of 3.4 s. The accumulation time was set to 0.025 s, except for fragmentation analyses with a 1 s accumulation period, both at a flow rate of 400 µL.h^{-1}. The electrospray ionization conditions were set as follows: desolvation gas flow, 4 L.min^{-1}; source temperature, 146 °C; source cone, 50 V; capillary voltage, -4500 V; nebulizer pressure, 0.5 bar; octopole energy, 350 V_{pp}; quadrupole lower cut-off, *m/z* 200; quadrupole collision energy, 1200 V_{pp}; TOF duration, 0.8 ms. A blank spectrum was recorded for 2 min prior to each sample introduction.

A hybrid quadrupole time-of-flight mass spectrometer, which incorporates a traveling wave (T-Wave)-based mobility separation device (Synapt G2-Si HDMS, Waters Corp., Manchester, U.K) was used to obtain ion mobility data. The instrument and the T-Wave device have been described in detail elsewhere.[38] Mass spectra were acquired in positive mode over *m/z* 50−1200 range for 20 min except for MS/MS (isolation/fragmentation) analyses which were conducted for 10 min. The high-resolution mode (W reflectron) was used yielding a resolution of 40000. All analyses were performed in triplicate to validate the repeatability of the experiments. The electrospray ionization conditions were set as follows: desolvation gas flow, 800 L.h^{-1}; source temperature, 120 °C; desolvation temperature, 300 °C. Capillary voltage was set at 2.5 kV; sampling cone, 50 V; and extraction cone, 5 V. The IMS parameters were: IMS gas flow, 90 mL.min^{-1} of N_2 (2.96 mbar of N_2 IMS cell pressure); IMS traveling wave height and velocity 40 V and 800 m.s^{-1}.

IMS cell calibration was performed with a solution of D/L polyalanine at a concentration of 10 ng.µL^{-1} in MeCN/H_2O as described by Smith et al.[45] Polyalanines CCS values used for calibration were taken from Pr. Clemmer CCS database.[46]

Mass spectrometers were externally *m/z* calibrated using sodium formate solution or sodium trifluoroacetate solution before sample analyses. Instrument control and data acquisition were provided by DataAnalysis (version 4.4) and MassLynx (version 4.1) software for the FTICR and Synapt G2-Si HDMS, respectively. DriftScope (version 2.2) was used for display and analysis of the ion mobility data, whereas OriginPro (version 2016) was used to process and visualize the data sets.
From the molecular formulas determined from the accurate mass measurements (typically <0.2 ppm), the number of double bond equivalents (DBE) values can be calculated utilizing Equation 1 (c: carbon number; h: hydrogen number; n: nitrogen number) for a molecular formula of $C_cH_hN_nO_oS_s$.[33, 34]. Given the resolving power of 0.9 10^6 at *m/z* 400 for the FTICR instrument, it is possible to separate N_1 class ions from class N_1S_1 (mass split: 3.4 mDa) compounds.

$$DBE = c - \frac{h}{2} + \frac{n}{2} + 1 \qquad \textit{Equation 1}$$

Results and Discussion

Broadband FTMS analysis

The positive ion mode ESI FTICR MS spectra of the feed (VGO) and the two effluents from HDN process containing 70 and 10 ppm nitrogen are presented Figure S1. The first observation is the significant decrease in the abundance and number of ions detected between the VGO and the effluents as for the deeply denitrogenated sample, chemical noise signals became predominant. As positive ESI mode was used, mainly basic nitrogen-containing species were detected. Figure 1 shows the DBE/C# maps of this N_1 family.

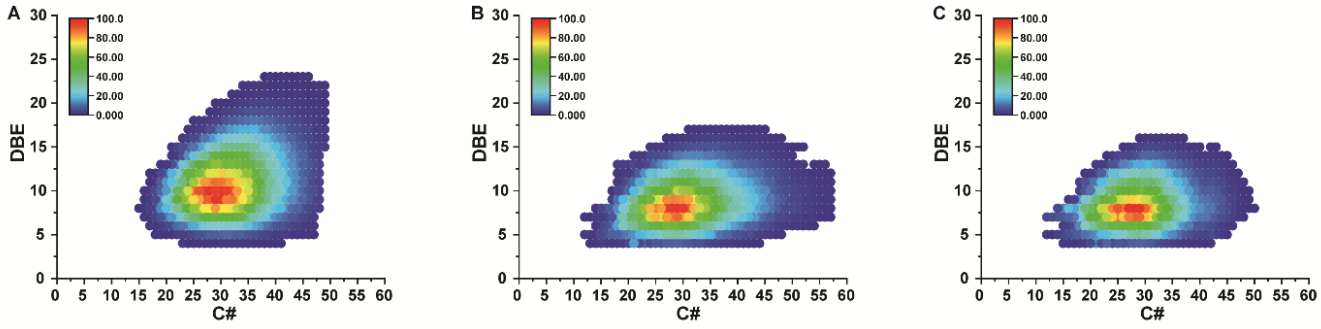

Figure 1. N_1 class DBE/C# maps of the feed VGO (A), Effluent 70 ppm (B) and Effluent 10 ppm (C) obtained from the ESI (+) experiments by FTICR MS

The most abundant compounds of the VGO N1 family can be found between C28 and C32 and DBE values between 8 and 11. The predominant components of the N_1 class for the 70 ppm effluent are slightly lower and were observed between C24 and C35 and DBE values between 8 and 9. Finally, the prevailing nitrogen compounds detected in the 10 ppm effluent are between C19 and C30, for DBE values between 7 and 9. Thus, it appears that following the hydrotreating process, the most refractory nitrogen compounds detected in ESI(+), corresponding to polyaromatic quinoline compounds. The change in the chemical pattern of the N_1 class between the VGO and the 70 ppm and 10 ppm effluents is relatively week and involves mainly the decline of high DBE molecules and a slight diminution of the average mass distribution. More significant differences between the samples may be found in the isomeric composition. For this purpose, MS/MS and IMS techniques can be considered.

Ultra high-resolution tandem mass spectrometry

In order to obtain further structural information, tandem mass spectrometry (MS/MS) experiments were performed on selected class N_1 ions. The ion at *m/z* 378.31553 ($C_{27}H_{40}N^+$, DBE 9) was investigated as it is the most abundant refractory compound representative in the 70 and 10 ppm effluents for the DBE 9 series. The *m/z* selection is performed with a quadrupole using the smallest achievable window of 1 *m/z* unit, limited by hardware itself. Thus, several isobaric ions are isolated within this selection window, belonging to N_1, N_1S_1, and N_1O_1 class constituents. Raw data extracted from the molecular attribution of the peaks of each spectrum have been filtered to focus only on class N_1 species. For the selected nominal masses investigated within this study, two isobaric compounds of class N_1 were detected. Consequently, when selecting the *m/z* 378 ions, the isobaric ions *m/z* 378.31553 ($C_{27}H_{40}N^+$, DBE 9) and *m/z* 378.22163 ($C_{28}H_{28}N^+$, DBE 16) are co-selected simultaneously (Figure 2); fragmentation will, therefore, occur on these two compounds. In order to visualize these isolation and fragmentation data, DBE/C# maps were drawn

(Figure 2) similar to the approach for the broadband spectra. In this case, the fragment ions of each isobar were detected along two different horizontal lines at DBE corresponding to n+1 with respect to the precursor ion, shown in Figure 3.[37, 47]

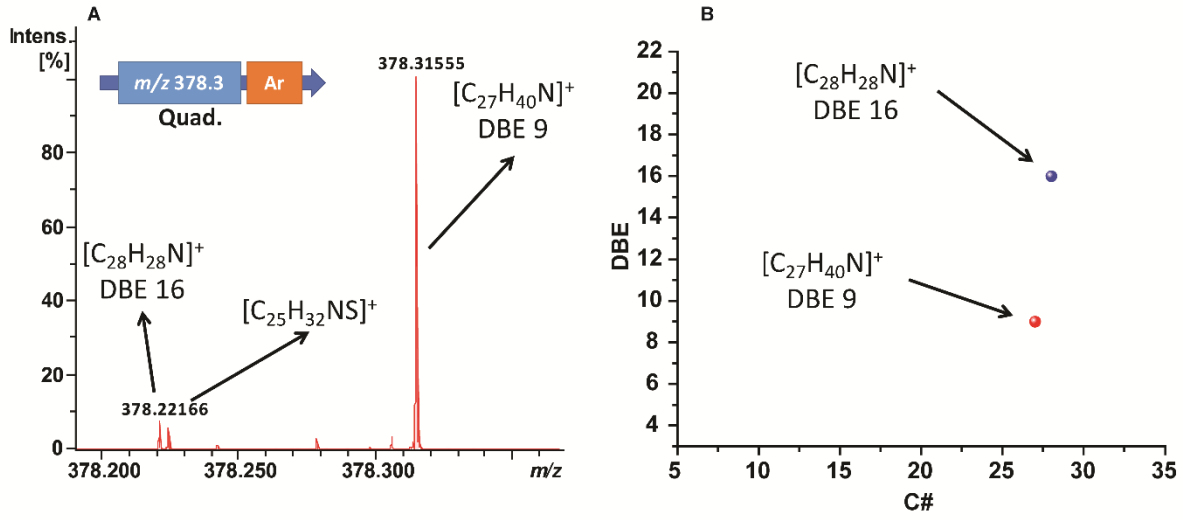

Figure 2. A) Expansion of the unit isolated window at *m/z* 378 showing the different isobaric ions that cannot be separated by the quadrupole, and B) transfer of the isobaric information of class N_1 to a DBE/C# map .

Figure S2 shows the MS/MS spectra of *m/z* 378 ions (most abundant ion *m/z* 378.31553 ($C_{27}H_{40}N^+$, DBE 9)) at different collision energies: 30 eV, 40 eV, 50 eV and 60 eV. Relatively high collision energies were required to generate fragment ions which highlight the high stability of these ions. Figure 3 shows the evolution of this fragmentation as a function of collision energy. A bimodal distribution of fragments is observed starting from the 40 eV spectrum, but more precisely on the 50 and 60 eV spectra, corresponding to the fragmentation pattern of the both co-isolated ions *m/z* 378.31553 ($C_{27}H_{40}N^+$, DBE 9) and *m/z* 378.22166 ($C_{28}H_{28}N^+$, DBE 16). From MS/MS experiments, fragment distribution can be used to reconstruct precursor oil molecules. The main limitation of this work is that the ions of the CID product cannot be directly correlated with the individual precursor ions.[26] It is therefore difficult to monitor CID mechanisms and draw conclusions about fragmentation patterns that change with the characteristics of precursor ions.[23, 48]

Figure 3 visualizes the DBE/C# maps for the respective fragment pattern of the precursor ion *m/z* 378.31553 ($C_{27}H_{40}N^+$, DBE 9) and *m/z* 378.22166 ($C_{28}H_{28}N^+$, DBE 16) at different collision energies from 30 eV to 60 eV. The main fragment ion series for both precursor corresponds to losses of small alkane molecules that involve a hydrogen transfer during the fragmentation mechanism.[37, 47] Consequently, this product ion series has a DBE of 10 and 17 involving an increase of the DBE value by one due to the displacement of the proton following the loss of the alkyl chain. It appears therefore that at a moderate collision energy value (30 eV), there was mainly a decrease in the carbon number (C#) with no change in DBE. This is consistent with competitive fragmentation processes involving alkane losses through alkyl chain cleavages.[23] On the other hand, with a higher collision energy value (60 eV), a decrease in DBE values was observed in addition to a decrease in carbon number that is probably related to consecutive processes involving ring opening reactions. The aromatic rings are very stable so this should be in particular possible with core structures featuring naphthenic motives. Retro-Diels-Alder processes may be involved among other fragmentation pathways, especially with tetralin core structures. These results imply that the losses of DBE observed at higher collision energy are consecutive fragmentations processes taking place after the losses of the alkyl chains. This is possible only if we assume island type molecules with fused core structure surrounded by alkyl chains.[23, 49-52]

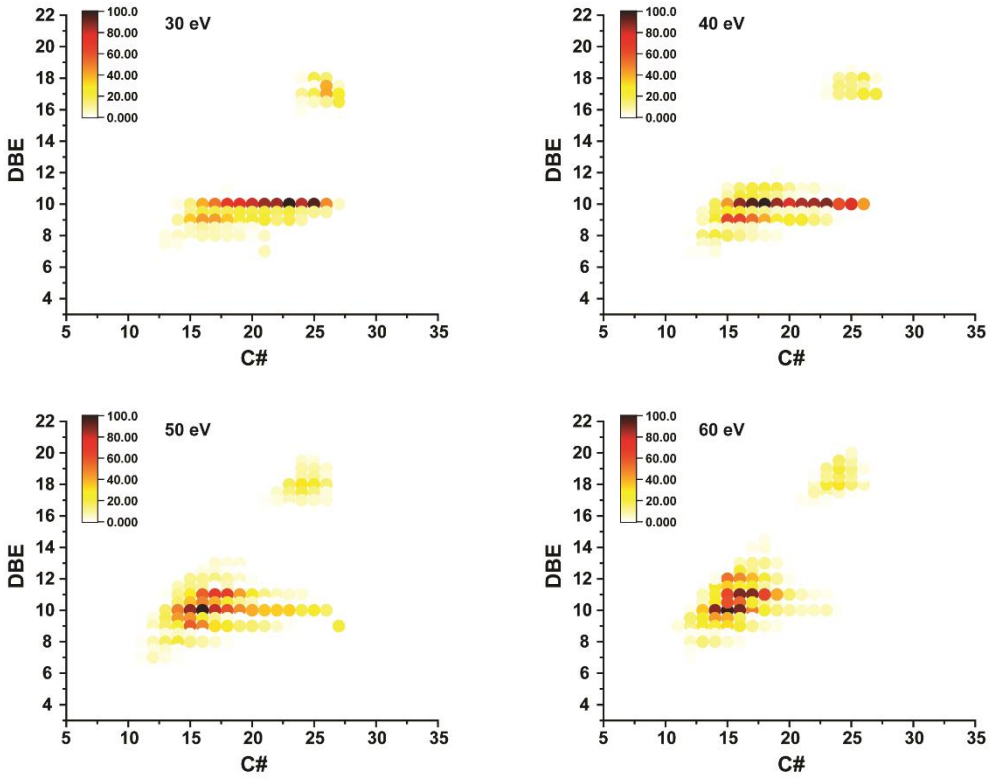

Figure 3. DBE/C# maps from the MS/MS spectra of *m/z* 378.31553 ($C_{27}H_{40}N^+$, DBE 9) and *m/z* 378.22166 ($C_{28}H_{28}N^+$, DBE 16) as a function of the collision energy value (30-60 eV).

The most intense fragment series from the two N1 ions isolated in the quadrupole, respectively at DBE 10 and 17, are plotted on a histogram graph according to their carbon number (Figure 4). For a specific DBE value, the series of fragment ions is following the same trend: a monomodal distribution with a specific maximum abundance at a certain carbon number. This maximum corresponds to the most stable fragment before obtaining consecutive fragments with DBE losses. Therefore, it is likely that this point corresponds to the molecular nucleus that presumably lost all its alkyl chains. The diminution of the ion abundance at lower C# can be rationalized by considering that once all alkyl chains are lost, consecutive fragmentation takes place involving dissociation of naphthenic rings on the core.

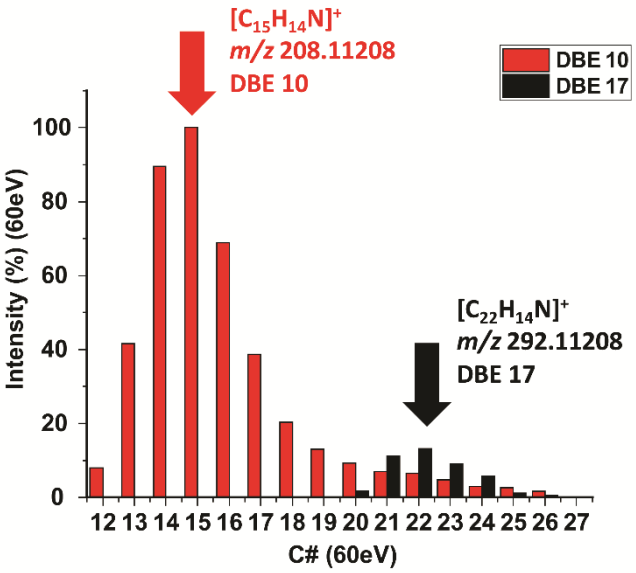

Figure 4. Histogram of fragment ions of $C_{27}H_{40}N^+$ and $C_{28}H_{28}N^+$ precursor ions as a function of their relative intensity with a collision voltage value of 60 eV

In this case, the major fragment ions, *m/z* 208.11208 ($C_{15}H_{14}N^+$, DBE 10) and *m/z* 292.11208 ($C_{22}H_{14}N^+$, DBE 17) should represent the dominant molecular nuclei of the isobar precursor ions, respectively *m/z* 378.31553 ($C_{27}H_{40}N^+$, DBE 9) and *m/z* 378.22163 ($C_{28}H_{28}N^+$, DBE 16) previously isolated in the quadrupole.

The evolution of the fragmentation of the basic nitrogen protonated molecules revealed a class of compounds allowing the identification of the molecular nucleus of petroleum compounds, as well as the understanding of the fragmentation pathways (by the loss of the alkyl chain in a first step, the opening and rearrangement of the nuclei thereafter).[26]

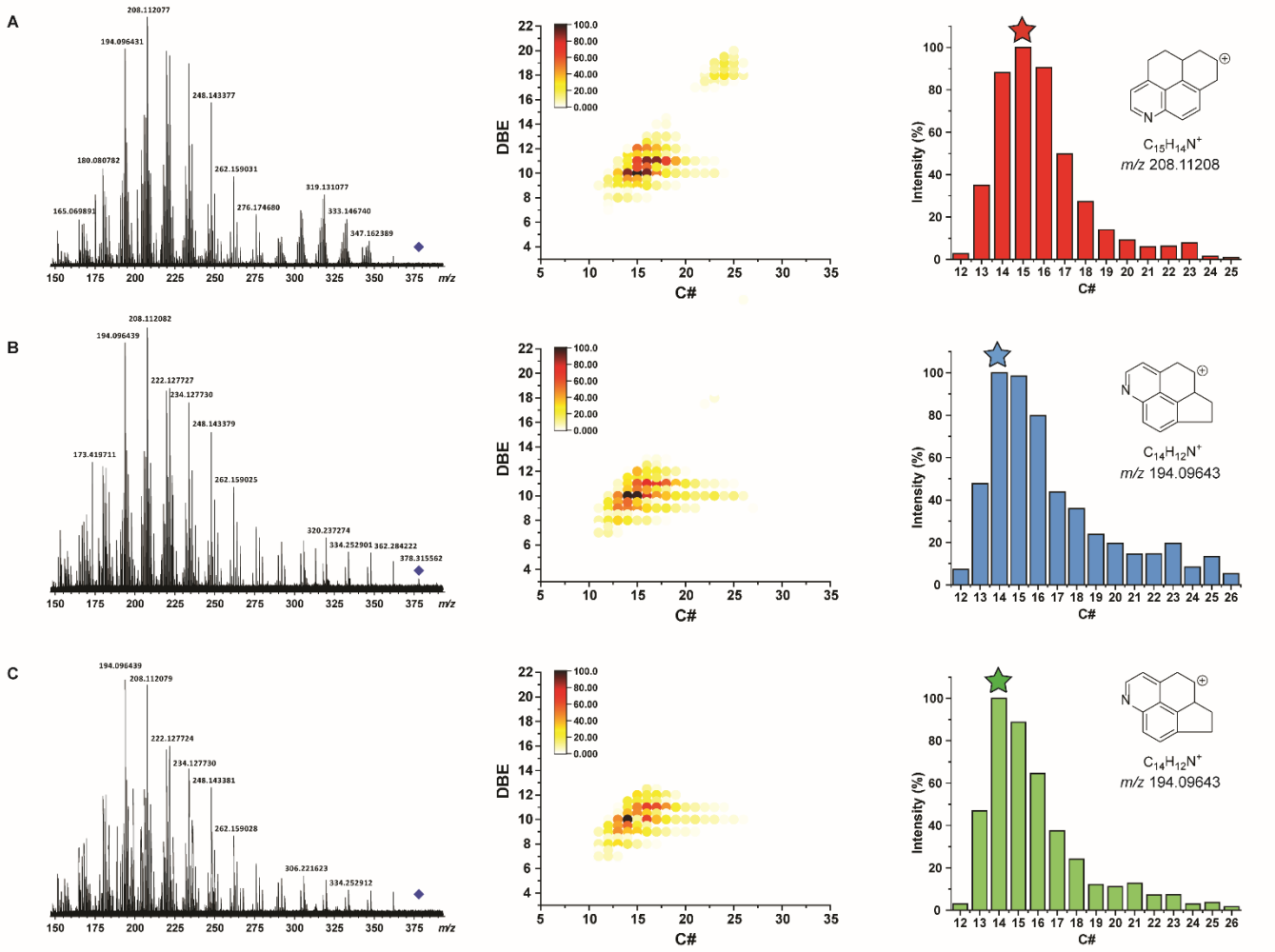

Figure 5. Fragmentation pattern of precursor ions *m/z* 378.31553 ($C_{27}H_{40}N^+$, DBE 9) and *m/z* 378.22166 ($C_{28}H_{28}N^+$, DBE 16) at a collision energy of 60 eV for A) VGO, B) Effluent 70 ppm, and C) Effluent 10 ppm.

Subsequently, the structural determination of the molecular core of the *m/z* 378.31555 ($C_{27}H_{40}N^+$, DBE 9) was also performed on the 70 and 10 ppm effluents. This made it possible to monitor the evolution of the refractory compound after the nitrogen removal treatment, shown in Figure 5. Interestingly, the identified fragments are identical to those observed for the VGO, but not at the same proportions. DBE/C# maps indicate that the most stable fragment found in the effluents is *m/z* 194.09643 ($C_{14}H_{12}N^+$, DBE 10). This could indicate a new type of molecular core resistant to the hydrodenitrogenation process. Figure S3 gives hypothetical molecular nucleus structures from the raw formula determined by the tandem mass spectrometry. The MS/MS experiments made it possible to determine the raw formula of the molecular nucleus and to tentatively identify the structures of these nuclei: "island" (central nucleus branched by alkyl chains) or "archipelago" (several central nuclei connected by an alkyl chain). In this case, the "island" structures were revealed predominantly. The types of archipelagos, if any, are only visible after the samples have been prepared to isolate them, because their ionization efficiency is much lower. The archipelago types form nanoaggregates much more than island types and are therefore not ionized.[28, 29]

Addition of an ion mobility separation dimension to separate isomeric compounds/fragments from these complex mixtures would allow to further identify the different conformations and reveal typical fragments of these molecular nuclei.[22]

Ion mobility spectrometry

The FTICR analysis using the MS/MS method enabled the identification of the molecular core structures based on the high mass resolving power and high mass accuracy. However, the mass spectrometry technique alone limits the understanding of isomers and does not allow to draw conclusions on the comparison of refractory compounds between the feed VGO and the effluents.

This is where ion mobility spectrometry is beneficial as it allows the separation of isomers.[40, 53-55] This technique can be applied on both precursor and product ions yielding various factors such as full width at half maximum (FWHM), drift time (t_D) and CCS (collision cross section).[45, 56] CCS represents the ability of an ion to be involved in collisions, so the more compact the conformation of an ion, the less likely it is to have collisions, and therefore the lower its CCS will be. Conversely, an unfolded conformation ion will have a higher CCS because it will have a greater collision probability. A compact conformation ion is, therefore, be characterized by a low CCS value, and will present a lower drift time as it reaches the detector faster compared to a less compact ion.
The resolution of the ion mobility is far too low to separate all isomers and, thus, the FWHM can be used as a descriptor of the isomeric content of a particular molecular formula.[37] The larger the width at half height, the greater the isomeric dispersity. Another descriptor of the isomeric dispersity is the drift time of this ion mobility profile that is representative of the average CCS of the detected isomers.

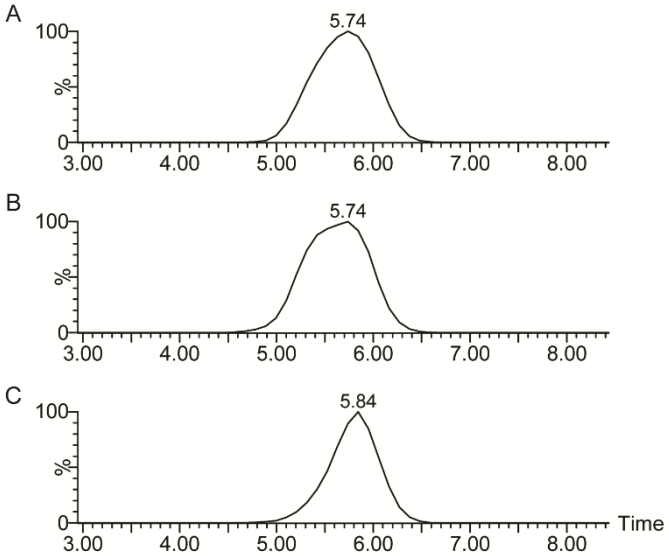

Figure 6. Ion mobility spectra of the *m/z* 378.31553 ($C_{27}H_{40}N^+$, DBE 9) selected in the quadrupole for A) VGO, B) effluent 70 ppm, and C) effluent 10 ppm .

The ion mobility spectra of the precursor ion at *m/z* 378.31553 ($C_{27}H_{40}N^+$, DBE 9) for the VGO before (A) and after mild (B) and deep (C) HDN processes are presented Figure 6. A significant change in the ion mobility peak profile is observed between the VGO and the deep HDN effluent as the latter presents a significantly higher drift time and lower FWHM. The effluent with 70 ppm (mild HDN) presents only a slight change of the signal profile with a lower amount of low drift time species. Interestingly, there is a significant increase of the drift time and CCS values for 10 ppm refractory ion, indicating the presence of less compact compounds. Illustrated differently, Figure S4 shows the evolution of the isobars ion mobility spectra at *m/z* 378 for the VGO before and after mild and deep HDN process. This same trend is observed on other examples of ions of class N_1 to *m/z* 380.331177 ($C_{27}H_{42}N^+$, DBE 8) and *m/z* 382.346827 ($C_{27}H_{44}N^+$, DBE 7), illustrated in Figure S5. As the HDN process progresses, the FWHM of the precursor mobility peak decreases indicating a decrease in the number of isomers. Furthermore, an increase in drift time is observed, reflected in the peak apex value, indicating the presence of compounds with higher CCS.

Table 1. Ion mobility descriptors of the refractory precursor ion isolated in the quadrupole.

	$C_{27}H_{40}N^+$ *m/z* 378.31553		
	t_D (ms)	FWHM (ms)	CCS (Å²)
VGO	5.70 ± 0.01	0.63 ± 0.01	137.9 ± 0.3

Effluent 70 ppm	5.62 ± 0.02	0.66 ± 0.01	136.5 ± 0.3
Effluent 10 ppm	5.81 ± 0.02	0.49 ± 0.01	140.3 ± 0.1

Table 1 reports the results of drift time and FWHM measurements after a Gaussian fit, as well as the CCS values calculated from the drift time values of the precursor refractory ions, selected in the quadrupole for the three samples. In each case, a decrease in the FWHM between the VGO and the 10 ppm effluent is observed. This indicates a decrease in isomeric variability after HDN treatment.[37, 57, 58] On the other hand, there is an increase in the value of CCS and drift time for each refractory precursor. This may indicate that basic nitrogen molecules with larger conformations are more resistant to hydrodenitrogenation processes. This can be due to the presence of different core structures or due to longer alkyl chains as shown previously in the discussion of the FTMS results.[37]

In a second stage, we were interested in the ion mobility spectrometry study of the refractory core fragments previously determined *via* the structural study by CID on the FTICR. The ion mobility spectra of the main fragment ion *m/z* 208.11208 (($C_{15}H_{14}N^+$, DBE 10) resulting from the fragmentation of the precursor ion at *m/z* 378.31553 ($C_{27}H_{40}N^+$, DBE 9) for the VGO before and after mild and deep HDN processes are presented Figure S6. The refractory precursor in the VGO and effluents was fragmented in the collision cell (*Trap* cell) located before the ion mobility cell. This operating mode makes it possible to study the ion mobility of CID fragments.

Table 2. Ion mobility descriptors of fragment ion at *m/z* 208.11208 ($C_{15}H_{14}N^+$, DBE 10) from refractory precursor ions fragmented in the trap cell.

	$C_{15}H_{14}N^+$ *m/z* 208.11208		
	t_D (ms)	FWHM (ms)	CCS (Å²)
VGO	2.81 ± 0.02	0.17 ± 0.01	87 ± 1
Effluent 70 ppm	2.83 ± 0.01	0.17 ± 0.01	87.6 ± 0.2
Effluent 10 ppm	2.84 ± 0.02	0.17 ± 0.01	86 ± 1

Table 2 reports the results of drift time and FWHM measurements after a Gaussian fit, as well as the CCS values calculated from the drift time values of the fragment ion *m/z* 208.11208 ($C_{15}H_{14}N^+$, DBE 10) representing the molecular core of the refractory *m/z* 378.31553 ($C_{27}H_{40}N^+$, DBE 9) which has been studied previously in this article. These calculations indicate that there is no significant difference in CCS for the fragment $C_{15}H_{14}N^+$ between the feed and its effluents. The compact fragment has few conformational possibilities, which would explain this small variation in CCS between samples. Differences in CCS on the molecules are mainly due to change in the organization of alkyl chains (position and length). From these IMS data, it can be postulated that the high CCS values refractory molecules present long alkyl chains. Examples of structures are shown in Figure 7. Such long chains may, depending on their position on the molecule relative to the nitrogen atom, prevent efficient access to the catalyst active site.

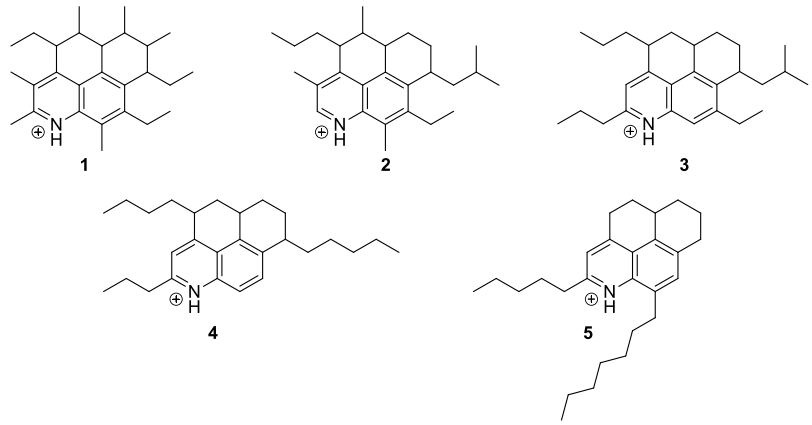

Figure 7. Examples of compact (1-3) and branched (4-5) structures of *m/z* 378.31553 ($C_{27}H_{40}N^+$, DBE 9)

Conclusions

The aim of this study was to identify and characterize compounds refractory to hydrodenitrogenation through the use of ultra-high-resolution tandem mass spectrometry and ion mobility spectrometry. The broadband FTICR MS data allowed to determine the basic compound family refractory to the HDN process which present mainly a DBE of 7, 8, and 9, and involved a partial removal of high DBE molecules. In fact, when comparing species with the same carbon number, those with a low DBE might exhibit a smaller molecular core and a higher amount of carbons as alkyl chains. From tandem mass spectrometry experiments, a putative structure of the ion refractory core was proposed based on the evolution of alkane losses from the protonated precursor ion as a function of the collision energy. This simplification facilitated a better understanding of the correlation between precursor and fragment ions and allowed differentiation between single and multi-core structures. Here, the obtained data are consistent with island core structures. A significant change in IMS profiles for the refractory precursor indicated that the isomers presenting high CCS values are more resistant to HDN processes. This should correspond to species presenting long branches compared to ramified molecules that should present lower CCS values. The combination of IMS-MS and ultra-high resolution spectrometry open up interesting and promising prospects for studies in the structural determination of complex mixtures, in particular, compounds that are problematic in different refining processes. It would be interesting in the future to add the ion mobility spectrometry separation dimension to ultra-high-resolution mass spectrometry (TIMS-FTICR) to separate isomeric compounds from these resistant species also for more complex mixtures and other ionisation techniques.

Conflicts of interest

There are no conflicts to declare

Acknowledgements

This work was supported by the European Regional Development Fund (ERDF) N°HN0001343, the European Union's Horizon 2020 Research Infrastructures program (Grant Agreement 731077), the Région Normandie, and the Laboratoire d'Excellence (LabEx) SynOrg (ANR-11-LABX-0029).

Notes and references

1. R. P. Rodgers and A. M. McKenna, *Analytical chemistry*, 2011, **83**, 4665-4687.
2. A. G. Marshall and R. P. Rodgers, *Proceedings of the National Academy of Sciences of the United States of America*, 2008, **105**, 18090-18095.
3. C. A. Hughey, R. P. Rodgers and A. G. Marshall, *Analytical chemistry*, 2002, **74**, 4145-4149.
4. C. A. Hughey, C. L. Hendrickson, R. P. Rodgers and A. G. Marshall, *Energy & Fuels*, 2001, **15**, 1186-1193.
5. C. A. Hughey, R. P. Rodgers, A. G. Marshall, C. C. Walters, K. Qian and P. Mankiewicz, *Organic Geochemistry*, 2004, **35**, 863-880.
6. C. M. Celis-Cornejo, D. J. Pérez-Martínez, J. A. Orrego-Ruiz and V. G. Baldovino-Medrano, *Energy Fuels*, 2018, **32**, 8715-8726.
7. A. Miyata, S. Omi and M. Nagai, *Journal of The Japan Petroleum Institute*, 1995, **38**, 251-257.
8. M. Lewandowski, *Applied Catalysis B: Environmental*, 2015, **168-169**, 322-332.
9. P. Benigni, R. Marin and F. Fernandez-Lima, *Int J Ion Mobil Spectrom*, 2015, **18**, 151-157.

10. H. Farag, M. Kishida and H. Al-Megren, *Applied Catalysis A: General*, 2014, **469**, 173-182.
11. S. Albersberger, J. Hein, M. W. Schreiber, S. Guerra, J. Han, O. Y. Gutiérrez and J. A. Lercher, *Catalysis Today*, 2017, **297**, 344-355.
12. X. Fan, G.-F. Liu, Z.-M. Zong, X.-Y. Zhao, J.-P. Cao, B.-M. Li, W. Zhao and X.-Y. Wei, *Fuel Processing Technology*, 2013, **106**, 661-665.
13. J. Ancheyta, 2016, DOI: 10.1002/9781118769638.
14. I. Mochida and K.-H. Choi, *Journal of the Japan Petroleum Institute*, 2004, **47**, 145-163.
15. Q. Shi, C. Xu, S. Zhao, K. H. Chung, Y. Zhang and W. Gao, *Energy & Fuels*, 2010, **24**, 563-569.
16. A. A. Al-Hajji, H. Muller and O. R. Koseoglu, *Oil & Gas Science and Technology - Revue de l'IFP*, 2008, **63**, 115-128.
17. L. A. Stanford, S. Kim, R. P. Rodgers and A. G. Marshall, *Energy Fuels*, 2006, **20**, 1664-1673.
18. J. Maillard, N. Carrasco, I. Schmitz-Afonso, T. Gautier and C. Afonso, *Earth. Planet. Sci. Lett.*, 2018, **495**, 185-191.
19. R. P. Rodgers and A. G. Marshall, 2007, DOI: 10.1007/0-387-68903-6_3, 63-93.
20. A. G. Marshall and T. Chen, *International Journal of Mass Spectrometry*, 2015, **377**, 410-420.
21. J. M. Purcell, C. L. Hendrickson, R. P. Rodgers and A. G. Marshall, *Anal Chem*, 2006, **78**, 5906-5912.
22. F. A. Fernandez-Lima, C. Becker, A. M. McKenna, R. P. Rodgers, A. G. Marshall and D. H. Russell, *Anal Chem*, 2009, **81**, 9941-9947.
23. A. M. Wittrig, T. R. Fredriksen, K. Qian, A. C. Clingenpeel and M. R. Harper, *Energy Fuels*, 2017, **31**, 13338-13344.
24. P. M. Lalli, J. M. Jarvis, A. G. Marshall and R. P. Rodgers, *Energy Fuels*, 2017, **31**, 311-318.
25. J. Bergquist, G. Baykut, M. Bergquist, M. Witt, F. J. Mayer and D. Baykut, *Int J Proteomics*, 2012, **2012**, 342659.
26. A. Vetere, W. Alachraf, S. K. Panda, J. T. Andersson and W. Schrader, *Rapid Commun Mass Spectrom*, 2018, DOI: 10.1002/rcm.8280.
27. T. Kekäläinen, J. M. H. Pakarinen, K. Wickström, V. V. Lobodin, A. M. McKenna and J. Jänis, *Energy & Fuels*, 2013, **27**, 2002-2009.
28. M. L. Chacón-Patiño, S. M. Rowland and R. P. Rodgers, *Energy Fuels*, 2017, **31**, 13509-13518.
29. M. L. Chacón-Patiño, S. M. Rowland and R. P. Rodgers, *Energy Fuels*, 2017, **32**, 314-328.
30. M. L. Chacón-Patiño, S. M. Rowland and R. P. Rodgers, 2018, **1282**, 113-171.
31. M. L. Chacón-Patiño, C. Blanco-Tirado, J. A. Orrego-Ruiz, A. Gómez-Escudero and M. Y. Combariza, *Energy Fuels*, 2015, **29**, 6330-6341.
32. C. A. Hughey, C. L. Hendrickson, R. P. Rodgers, A. G. Marshall and K. Qian, *Analytical Chemistry*, 2001, **73**, 4676-4681.
33. S. Kim, R. W. Kramer and P. G. Hatcher, *Anal. Chem.*, 2003, **75**, 5336-5344.
34. E.-K. Kim, M.-H. No, J.-S. Koh and S.-W. Kim, *Mass Spectrometry Letters*, 2011, **2**, 41-44.
35. C. P. Rüger, C. Grimmer, M. Sklorz, A. Neumann, T. Streibel and R. Zimmermann, *Energy & Fuels*, 2017, **32**, 2699-2711.
36. C. P. Rüger, A. Neumann, M. Sklorz, T. Schwemer and R. Zimmermann, *Energy & Fuels*, 2017, **31**, 13144-13158.
37. M. Farenc, B. Paupy, S. Marceau, E. Riches, C. Afonso and P. Giusti, *J Am Soc Mass Spectrom*, 2017, **28**, 2476-2482.
38. D. N. Mortensen, A. C. Susa and E. R. Williams, *J Am Soc Mass Spectrom*, 2017, **28**, 1282-1292.
39. J. G. Forsythe, A. S. Petrov, C. A. Walker, S. J. Allen, J. S. Pellissier, M. F. Bush, N. V. Hud and F. M. Fernandez, *Analyst*, 2015, **140**, 6853-6861.
40. S. Hupin, H. Lavanant, S. Renaudineau, A. Proust, G. Izzet, M. Groessl and C. Afonso, *Rapid commun. mass spectrom.*, 2018, DOI: 10.1002/rcm.8230.
41. X. Li, J. Zhu and B. Wu, *Bulletin of the Korean Chemical Society*, 2014, **35**, 165-172.
42. K. Qian, W. K. Robbins, C. A. Hughey, H. J. Cooper, R. P. Rodgers and A. G. Marshall, *Energy & Fuels*, 2001, **15**, 1505-1511.
43. Q. Shi, S. Zhao, Z. Xu, K. H. Chung, Y. Zhang and C. Xu, *Energy Fuels*, 2010, **24**, 4005-4011.
44. M. Farenc, Y. E. Corilo, P. M. Lalli, E. Riches, R. P. Rodgers, C. Afonso and P. Giusti, *Energy Fuels*, 2016, **30**, 8896-8903.
45. D. P. Smith, T. W. Knapman, I. Campuzano, R. W. Malham, J. T. Berryman, S. E. Radford and A. E. Ashcroft, *Eur J Mass Spectrom (Chichester)*, 2009, **15**, 113-130.
46. http://www.indiana.edu/~clemmer/Research/CrossSectionDatabase/Peptides/polyaminoacid_cs.htm.
47. J. D. Ciupek, D. Zakett, R. G. Cooks and K. V. Wood, *Analytical Chemistry*, 2002, **54**, 2215-2219.
48. C. S. Ling Liu, Songbai Tian, Qundan Zhang, Xinheng Cai, Yingrong Liu, Zelong Liu, Wei Wang, *Fuel*, 2018, DOI: https://doi.org/10.1016/j.fuel.2018.11.130.
49. K. Miyabayashi, Y. Naito, K. Tsujimoto and M. Miyake, *Journal of the Japan Petroleum Institute*, 2004, **47**, 326-334.
50. Z. H. Linzhou Zhang, Scott R Horton, Michael T Klein, Quan Shi, Suoqi Zhao, and Chunming Xu, 2013.
51. D. J. Porter, P. M. Mayer and M. Fingas, *Energy Fuels*, 2004, **18**, 987-994.
52. L. Zhang, Y. Zhang, S. Zhao, C. Xu, K. H. Chung and Q. Shi, *Science China Chemistry*, 2013, **56**, 874-882.
53. A. A. Shvartsburg and R. D. Smith, *Anal Chem*, 2008, **80**, 9689-9699.
54. K. Giles, J. P. Williams and I. Campuzano, *Rapid Commun. Mass Spectrom.*, 2011, **25**, 1559-1566.
55. A. M. Hamid, Y. M. Ibrahim, S. V. Garimella, I. K. Webb, L. Deng, T. C. Chen, G. A. Anderson, S. A. Prost, R. V. Norheim, A. V. Tolmachev and R. D. Smith, *Anal Chem*, 2015, **87**, 11301-11308.
56. C. Kune, J. Far and E. De Pauw, *Anal Chem*, 2016, **88**, 11639-11646.
57. A. L. Mendes Siqueira, M. Beaumesnil, M. Hubert-Roux, C. Loutelier-Bourhis, C. Afonso, Y. Bai, M. Courtiade and A. Racaud, *J Am Soc Mass Spectrom*, 2018, **29**, 1678-1687.
58. A. L. Mendes Siqueira, M. Beaumesnil, M. Hubert-Roux, C. Loutelier-Bourhis, C. Afonso, S. Pondaven, Y. Bai and A. Racaud, *Analyst*, 2018, **143**, 3934-3940.